



Groundwater Quality Evaluation of Fractured Aquifers Using Machine Learning Models and Hydrogeochemical Approaches to Sustainable Water-Irrigation Security in Arid Climate (Central Tunisia)

Mohamed Haythem Msaddek, Yahya Moumni, Lahcen Zouhri, Ismail Chenini,
Adel Zghibi

► To cite this version:

Mohamed Haythem Msaddek, Yahya Moumni, Lahcen Zouhri, Ismail Chenini, Adel Zghibi. Groundwater Quality Evaluation of Fractured Aquifers Using Machine Learning Models and Hydrogeochemical Approaches to Sustainable Water-Irrigation Security in Arid Climate (Central Tunisia). *Water*, 2023, 15 (19), pp.3332. 10.3390/w15193332 . hal-04218337

HAL Id: hal-04218337

<https://normandie-univ.hal.science/hal-04218337>

Submitted on 26 Sep 2023

HAL is a multi-disciplinary open access archive for the deposit and dissemination of scientific research documents, whether they are published or not. The documents may come from teaching and research institutions in France or abroad, or from public or private research centers.

L'archive ouverte pluridisciplinaire **HAL**, est destinée au dépôt et à la diffusion de documents scientifiques de niveau recherche, publiés ou non, émanant des établissements d'enseignement et de recherche français ou étrangers, des laboratoires publics ou privés.

Article

Groundwater Quality Evaluation of Fractured Aquifers Using Machine Learning Models and Hydrogeochemical Approaches to Sustainable Water-Irrigation Security in Arid Climate (Central Tunisia)

Mohamed Haythem Msaddek ^{1,*}, Yahya Moumni ^{1,2}, Lahcen Zouhri ³, Ismail Chenini ¹ and Adel Zghibi ^{1,4}

¹ LR01ES06 Laboratoire des Ressources Minérales et Environnement, Faculté des Sciences de Tunis, Université de Tunis El Manar, Tunis 2092, Tunisia; yahya.moumni@fsb.ucar.tn (Y.M.); ismail.chenini@fst.utm.tn (I.C.); azghibi@hbku.edu.qa (A.Z.)

² Department of Earth Sciences, Faculty of Sciences of Bizerte, University of Carthage, Bizerte 7120, Tunisia

³ AGHYLE, Institut Polytechnique UniLaSalle Beauvais, SFR Condorcet FR CNRS 3417, 19 Rue Pierre Waguet, 60026 Beauvais, France; lahcen.zouhri@unilasalle.fr

⁴ College of Science and Engineering, Hamad Bin Khalifa University, Qatar Foundation, Doha P.O. Box 34110, Qatar

* Correspondence: haythem.msaddek@fst.utm.tn



Citation: Msaddek, M.H.; Moumni, Y.; Zouhri, L.; Chenini, I.; Zghibi, A. Groundwater Quality Evaluation of Fractured Aquifers Using Machine Learning Models and Hydrogeochemical Approaches to Sustainable Water-Irrigation Security in Arid Climate (Central Tunisia). *Water* **2023**, *15*, 3332. <https://doi.org/10.3390/w15193332>

Academic Editor: Aldo Fiori

Received: 29 August 2023

Revised: 20 September 2023

Accepted: 21 September 2023

Published: 22 September 2023



Copyright: © 2023 by the authors. Licensee MDPI, Basel, Switzerland. This article is an open access article distributed under the terms and conditions of the Creative Commons Attribution (CC BY) license (<https://creativecommons.org/licenses/by/4.0/>).

1. Introduction

Groundwater plays a vital role as a significant water resource in a nation's journey towards socioeconomic advancement. In contrast, agriculture stands out as the largest consumer of groundwater on a global scale [1–3]. Especially in areas characterized by dry and semi-dry conditions, the accessibility of irrigation water plays a crucial role in shaping agricultural productivity and the enlargement of cultivated areas. This, in turn, exerts a considerable influence on the sustainability of crop productivity. Nonetheless, these invaluable water sources face an array of challenges arising from environmental factors, human interventions, and natural phenomena [1,4,5]. The collective impact of these factors

leads to a decline in the chemical and physical attributes of groundwater, rendering it inadequate for agricultural use.

However, active and disused mines generate significant discharge, rock debris, and tailings. Within these waste materials, a sequence of intricate physical-chemical processes, including weathering, dissolution, and oxidation, occur, along with the leaching and erosion caused by groundwater and surface runoff. These processes result in the formation of mine drainage characterized by elevated levels of sulfate and heavy metals in its mineralogical composition. The movement of these dissolved and drained metals has a profound impact on the initial geochemical setting, leading to heavy metal contamination and the degradation of groundwater and soil quality within mining regions [6,7]. Moreover, the contamination consequences and the accumulation of heavy metals pose significant hazards to humans and other organisms residing in close proximity to mining regions [6–9].

Groundwater chemistry investigations have found extensive application in assessing water quality. Consequently, the presence of physicochemical components in irrigation water can have detrimental effects on both crop productivity and soil health [5,6]. Across various hydrogeochemical investigations, a range of water quality metrics have been compared against established standards to evaluate the groundwater's quality. However, this method falls short of providing decision-makers with instant insights and a comprehensive comprehension of groundwater quality, especially when multiple factors contributing to the deterioration of water quality are identified. To address this limitation, various computer-assisted plotting techniques like Piper, Durov, Schofield, Wilcox, and United States Salinity Laboratory (USSL) approaches have been involved in assessing the appropriateness of groundwater for agricultural watering [10–17]. Furthermore, Integrated Irrigation Groundwater Quality Indices (IIGWQIs) are derived from water's chemical composition and offer an effective means of evaluating water suitability. By amalgamating several pivotal water quality indicators into a single value, these indices are designed to facilitate water quality management decisions for stakeholders [10,11,15,18–21]. In the context of agriculture, these IIGWQIs are typically evaluated using a range of indices and variables [15,18,19]. Notably, the Irrigation Water Quality Index (IWQIndex), Sodium Adsorption Ratio Index (SARIndex), Soluble Sodium Percentage Index (SSPIndex), Potential Salinity Index (PSIndex), Kelley Index (KIndex), and Residual Sodium Carbonate Index (RSCIndex) are frequently employed to classify the appropriateness of groundwater for agricultural watering. These indicators help establish the ability of the rock formation to absorb water [15,22–25]. Across the globe, numerous studies have leveraged Integrated Irrigation Groundwater Quality Indices (IIGWQIs) in conjunction with GIS technology to assess groundwater's fitness for agricultural purposes. This approach enables the delineation of quality zones for irrigation through the generation of groundwater quality maps [18–25].

The assessment of irrigation water quality using traditional methods for agricultural production often proves to be both costly and time-intensive. However, this challenge can be effectively addressed by employing Machine Learning techniques to evaluate and predict Integrated Irrigation Groundwater Quality Indices (IIGWQIs) based on physico-chemical parameters. Examples of such techniques include the application of Least-Squares Support Vector Machines (LS-SVM) and Pearson Correlation Fuzzy Inference-based Systems (PC-FIS). Furthermore, the development of affordable and innovative technologies is imperative to establish sustainable, long-term strategies for managing groundwater quality. Effectively addressing this concern is crucial for ensuring robust environmental stewardship, particularly by anticipating variations in water quality indicators. Consequently, there has been a recent surge in the adoption of deterministic models within this domain [15–17,20,21,24,26–30].

In the realm of water quality modeling, certain characteristics often prove either prohibitively costly to measure or entirely beyond measurement capabilities [31,32]. In addressing water-related challenges, significant strides have been made in the advancement and utilization of Machine Learning tools. Operating without explicit knowledge of

the system's physical behavior, Machine Learning depends on scrutinizing the data that characterizes the system and skillfully emulating the intricate relationships among input and output variables [28]. Machine Learning simulation models incorporate an array of models, ranging from traditional statistical calculations like Auto-Regression Models (ARMs) and Moving Average Models (MA) to more sophisticated forms of Artificial Intelligence such as neural network prediction and support vector machine learning [31,32]. Notably, fuzzy neural network prediction models emerge as particularly potent within the Machine Learning paradigm. Renowned for their high predictive accuracy and adaptability, these models have found widespread application in addressing various challenges in water management [33–35]. Their efficacy lies in accurately simulating and estimating intricate hydrological data and nonlinear functions, proving especially effective for tasks like forecasting river inflows [33]. Another prominent Machine Learning approach is the support vector machine model, frequently harnessed for modeling hydrology datasets [34]. This method stands out in its ability to simplify the complexities of dynamic systems, capture nonlinear patterns, and gather the necessary data for well-informed decision-making with a remarkable level of accuracy [36]. The study area has witnessed a range of investigations focusing on diverse aspects, including monitoring water levels, assessing hydraulic parameters, evaluating health risks associated with drinking water, and tracking changes in soil quality over time.

To assess the effectiveness of the proposed approach within the context of an arid region, the Meknassy basin serves as a representative case study. This basin typifies an irrigated area in a mining environment situated in the arid climate of central Tunisia, where groundwater stands as the sole source for both irrigation and residential purposes.

This study aimed to accomplish the following primary goals: (i) characterize groundwater chemistry, categorize groundwater types, and elucidate the geochemical influences through the utilization of physical and geochemical elements and simulation methodologies; (ii) evaluate the appropriateness of groundwater for agricultural utilization using diverse Integrated Irrigation Groundwater Quality Indices (IIGWQIs); and (iii) scrutinize the efficacy of PC-FIS and LS-SVM models in accurately forecasting key IIGWQIs, including IWQIndex, SARIndex, SSPIIndex, PSIndex, KIndex, and RSCIIndex.

This study presents a novel approach to forecasting key indicators of interest in Groundwater Quality for irrigation purposes (IIGWQIs) under an arid climate case study by employing Least-Squares Support Vector Machines (LS-SVM) and the Pearson Correlation Fuzzy Inference-based System (PC-FIS) models. While previous research in similar case studies of arid areas has explored machine-learning algorithms for groundwater quality prediction, the specific application of PC-FIS and LS-SVM to IIGWQIs is relatively uncharted territory. Our study pioneers the use of these models in this context, showcasing their superior predictive performance compared to traditional methods [10,11,15,18–25]. Additionally, we contribute methodological insights into the configuration and optimization of these models for groundwater quality forecasting. This research holds practical significance for groundwater management and environmental protection, offering decision-makers a more accurate tool for assessing and mitigating water quality issues. We believe that the successful application of PC-FIS and LS-SVM models to IIGWQI forecasting sets a new benchmark for groundwater quality research and underscores the adaptability of advanced machine learning techniques in hydrogeology.

2. Study Area

The Meknassy region, encompassing an extent of 1235 km², serves as a representative example of a Mediterranean arid climate region. Its location lies within the southern central Atlas of Tunisia, known for extensive mining activities, especially phosphate and gypsum extraction [37]. This basin constitutes an independent hydrogeological unit [27,37] and is underpinned by a diverse array of geological formations. The characterization of the Meknassy basin's geology (Figure 1) is compiled by studying published geological maps and conducting firsthand observations on-site. This representation

showcases prominent outcroppings of fractured carbonates. Among these formations, the Mio-Plio-Quaternary segment displays variation in its composition, with varying granulometric compositions encompassing sandstone and gravel. Cretaceous formations exhibit a fracturing pattern on differing scales. Notably, the recent Quaternary deposits within the study region consist of permeable formations. The variation in the depth of the Mio-Plio-Quaternary sand and gravel accumulations primarily stems from irregularities in bedrock topography [27,37–42]. As one moves eastward within the study area, the depth of the phreatic aquifer increases [27,37], but its spatial extent remains constrained due to the surrounding elevations encompassing the hydrogeological basin. On average, the depth of this formation measures around 65 m. The shallow aquifer's porosity is estimated at 28% [37,38].

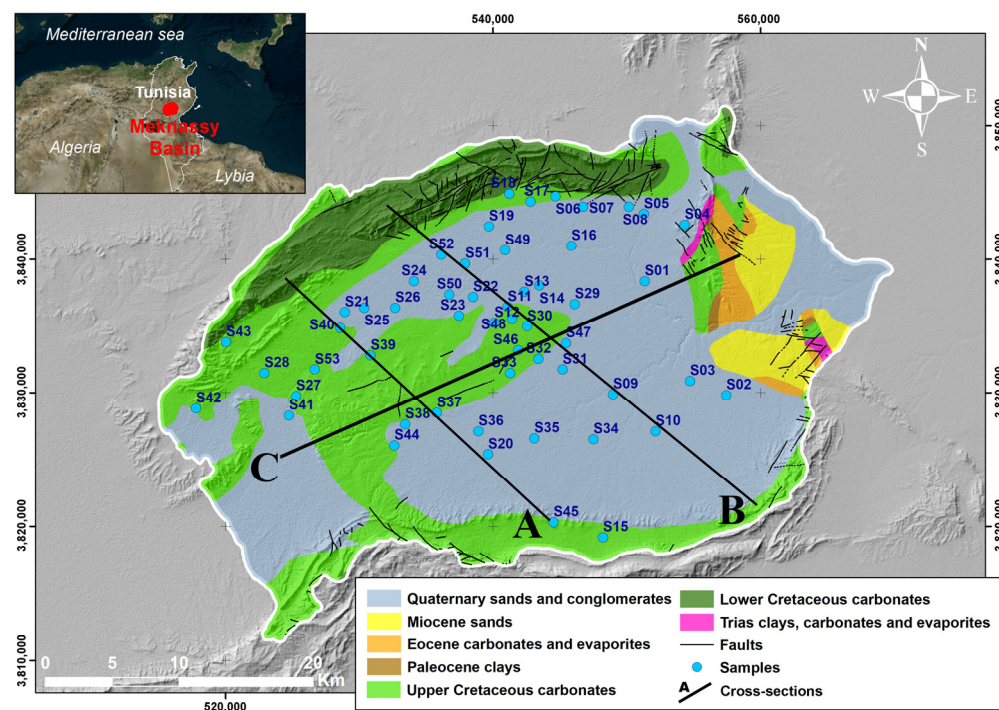


Figure 1. Map of the geological settings of the Meknassy basin.

In the principal outcrop regions of the hydrogeological Meknassy basin, the fractured formations have undergone secondary porosity development as a result of the fracturing and jointing processes. The Albian-Cenomanian Formation primarily consists of fractured carbonates, whereas the Late Turonian Formation is characterized by fractured dolomitic limestone. The upper level exhibits an average depth of approximately 155 m, with the lower level reaching depths of 285 m. Rainfall in the study area averages around 207 mm annually [27,37]. The boundaries of this region are defined by anticlinal folds that originated during compressive phases in the Miocene and Pleistocene periods [39,42].

The geological composition is distinguished by the occurrence of sedimentary deposits from the Mio-Plio-Quaternary period that delineate the near-surface aquifer. The fissured Cretaceous formations encompass the deep aquifer [37,38]. Within the study area, groundwater is predominantly found within weathered segments of rocks along joints and fractures, as well as within outcroppings of porous materials. Notably, groundwater movement was observed to predominantly follow an east-west direction, aligning with the gradual decline in topography.

The hydrogeological examinations conducted in the Meknassy basin reveal a partitioning of the study terrain into two distinct hydrogeological entities, recognized as aquifers with both permeable and fractured characteristics. The permeable aquifer encompasses the sedimentary deposits of sands and gravels from the Mio-Plio-Quaternary period, which define the shallow aquifer. Meanwhile, the fractured limestone water-bearing formation

is formed by the fractured limestone and dolomite formations from the late Cretaceous period. Notably, this fractured carbonate aquifer is especially notable as the primary aquifer of significant importance in the area.

In the relatively low-level stretches of the Meknassy basin, the sedimentary deposits of alluvial strata and Mio-Plio-Quaternary sand and gravel, which constitute the permeable aquifer, exhibit limited thickness. Various exploratory boreholes have been used to infer the stratigraphic cross-sections of this aquifer, as illustrated in Figure 2.

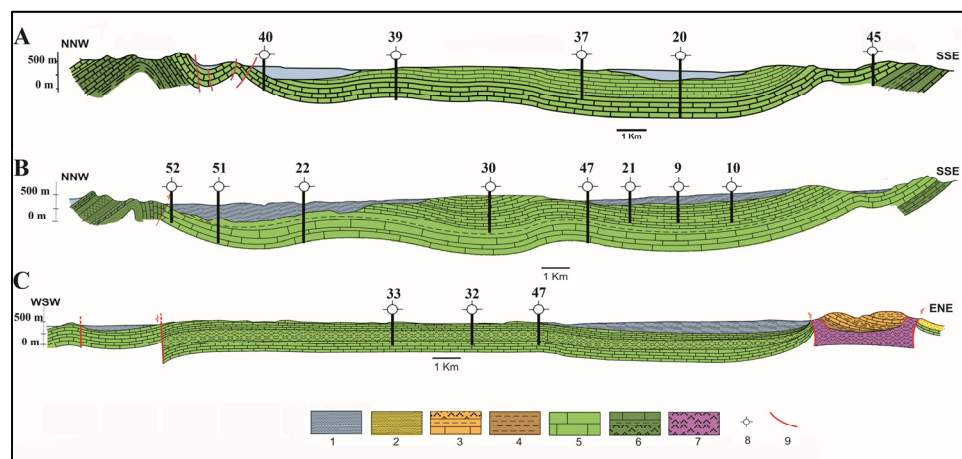


Figure 2. Cross-sections showing the subsurface characteristics of the Meknassy basin [27]: 1 Quaternary sands and conglomerates, 2 Miocene sands, 3 Eocene carbonates and evaporites, 4 Paleocene clays, 5 Upper Cretaceous carbonates, 6 Lower Cretaceous carbonates, 7 Trias clays, carbonates, and evaporites, 8 Sampling wells, and 9 Faults.

The fissured carbonate aquifer, which is the primary focus of this study, demonstrates varying hydraulic conductivity characteristics. Notably, To the west and within the encompassing mountainous regions, hydraulic conductivity is relatively high, surpassing 10^{-4} m/s. However, as one moves eastward within the study area, there is a progressive decline in hydraulic conductivity, resulting in lower values ranging from approximately 0.05 to 1×10^{-4} m/s.

The observation wells within the study region validate the prevailing pathway of subterranean water movement with W-E predomination. The depth of the water table exhibits variability, ranging from 30 m to 200 m (Figure 3a). The groundwater reserves within the fissured carbonate aquifer of the study locale display an annual utilization rate of 3.81 mm^3 per year, accompanied by a consistent theoretical discharge of 76 L/s. Furthermore, the collective salinity levels of the groundwater resources vary between 1.398 g/L and 4.469 g/L (Figure 3b).

The predominant direction of groundwater movement occurs from the western side towards the eastern region, following the drainage pathways within the Meknassy basin. The determination of the groundwater flow direction and recharge area was based on the overall hydrodynamic characteristics of the aquifer.

The residents of the Meknassy region, comprising approximately 60,000 individuals, grapple with contamination stemming from mining and open pit carrying activities, unregulated agricultural and extractive activities, and industrial processing operations [27]. Modern farming practices have significantly impacted the quality of water, primarily because of the utilization of chemical plant nutrients and crop protectants, leading to considerable contamination of this vital resource.

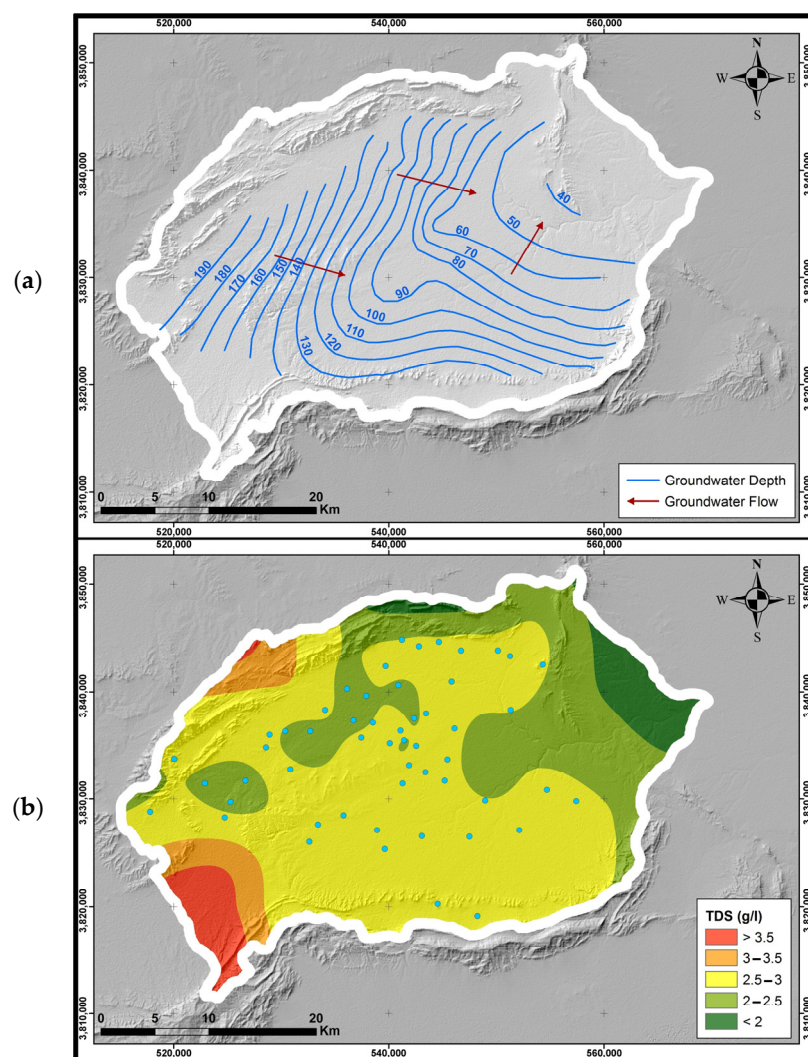


Figure 3. Groundwater characteristics of the Meknassy basin: (a) a spatial map of the piezometric level (2022) and (b) a map of the TDS concentration.

Prior to 1990, groundwater was primarily sourced from springs and shallow wells with free-flowing access, catering to extensive irrigation demands. Subsequently, there has been a continuous escalation in groundwater utilization, leading to a reduction in groundwater levels and requiring the drilling of deeper wells. The declining aquifer in the Meknassy basin has emphasized an urgent requirement for proficient control of groundwater withdrawal, as emphasized by various studies [27,37,38]. Additionally, a notable challenge in achieving management of groundwater resources lies in the scarcity of hydrogeological data essential for estimating groundwater flow patterns and anticipating the consequences of groundwater abstraction [27,37].

Hence, the Meknassy basin necessitates consistent surveillance and evaluation of irrigation water quality owing to its proximity to several phosphate mines and gypsum open pits. This imperative arises from the need to comprehend the potential ramifications of swift water level declines, geological makeup, and human interventions on irrigation water quality. Such insights are pivotal due to their subsequent impact on both soil quality and crop yield. Ultimately, the goal is to formulate well-informed suggestions for the responsible management of water resources in the Meknassy basin, guided by the principles embodied in Integrated Irrigation Groundwater Quality Indices (IIGWQIs) [15,18,19].

3. Compilation of a Hydrogeochemical Dataset

3.1. Groundwater Sampling, Gathering, and Analytical Assessment

The water sampling was procured in July 2022 from a total of 53 production wells (53 samples were collected), ranging in depths from 30 m to 200 m, thereby penetrating the fractured carbonate aquifer. On-site measurements encompassed parameters including temperature, TDS, pH, and electrical conductivity (ElC). ElC and pH were monitored using a portable multimeter. After filtration, each sample was carefully gathered using polyethylene containers for the purpose of examination of chemical constituents, specifically Ca^{2+} , Mg^{2+} , Na^+ , K^+ , Cl^- , HCO_3^- , and SO_4^{2-} . Spectrophotometry was employed for the analysis of SO_4^{2-} and Cl^- , while K^+ , Ca^{2+} , and Na^+ were quantified using a flame spectrophotometer. The method based on complexometric titration was utilized for the assessment of Mg^{2+} , while CO_3^{2-} and HCO_3^- were quantified through a titrimetric approach. To ensure accuracy, the Charge-Balance Error (CBE), limited to 5%, was employed as per Equation (1) to validate the accuracy of the analysis for ion concentrations calculated in meq/L.

$$\text{CBE} = \frac{\sum \text{Cations} - \sum \text{Anions}}{\sum \text{Cations} + \sum \text{Anions}} \times 100 \quad (1)$$

Quality control measures were implemented to establish the reliability of the examination methods, including thorough calibration of equipment and meticulous assessment of the precision of each analyzed sample.

3.2. The Indexing Method for Integrated Irrigation Groundwater Quality (IIGWQIs)

An exhaustive analysis of groundwater quality in relation to irrigation systems was conducted using the Integrated Irrigation Groundwater Quality Indices (IIGWQIs) approach. This process involves assessing groundwater quality for irrigation through the utilization of either individual hydrogeochemical indices or a combination of several indices, all facilitated by IIGWQIs [43,44]. While evaluating groundwater suitability for agricultural watering using specific criteria holds significance, amalgamated indexes offer more comprehensive insights of great importance to those making decisions. Assessing the suitability of groundwater for agricultural watering encompassed six distinct hazard categories, namely: (1) Irrigation Water Quality Index (IWQIndex), (2) Sodium Adsorption Ratio Index (SARIndex), (3) Soluble Sodium Percentage Index (SSPIndex), (4) Potential Salinity Index (PSIndex), (5) Kelley Index (KIndex), and (6) Residual Sodium Carbonate Index (RSCIndex).

3.2.1. Irrigation Water Quality Index (IWQIndex)

It is a unitless measure falling within the range of 0 to 100 and is determined derived from a collection of criteria that encompass Electrical Conductivity (ElC), Sodium Adsorption Ratio Index (SARIndex), as well as the concentrations of Na^+ , Cl^- , and HCO_3^{2-} [6,31,32]. The calculation is outlined in Equations (2) and (3) as follows:

$$\text{IWQIndex} = \sum_{i=1}^n \text{GWQ}_i \text{PW}_i \text{ (mg/L)} \quad (2)$$

The Groundwater Quality Index (GWQ_i) serves as a quantifiable measure of groundwater quality, grounded in tolerance thresholds, while PW_i represents the predefined weighting assigned to the individual parameters (Table 1).

$$\text{GWQ}_i = \text{GWQ}_{max} - \left(\frac{[(xy - V_{low}) \times \text{GWQ}_{rg}]}{V_{rg}} \right) \quad (3)$$

Table 1. The high and low boundaries of the parameters employed in the assessment of quality (GWQ_i) [43].

GWQ_i	EIC ($\mu\text{s}/\text{cm}$)	SARIndex	Na	Cl	HCO_3
0–35	EIC < 200 or EIC \geq 3000	SARIndex > 2 or SARIndex \geq 12	Na < 2 or SARIndex \geq 9	Cl < 1 or Cl \geq 10	$\text{HCO}_3 < 1$ or $\text{HCO}_3 \geq 8.5$
35–60	$1500 \leq \text{EIC} < 3000$	$6 \leq \text{SAR} < 12$	$6 \leq \text{Na} < 9$	$7 \leq \text{Cl} < 10$	$4.5 \leq \text{HCO}_3 < 8.5$
60–85	$750 \leq \text{EIC} < 1500$	$3 \leq \text{SAR} < 6$	$3 \leq \text{Na} < 6$	$4 \leq \text{Cl} < 7$	$1.5 \leq \text{HCO}_3 < 4.5$
85–100	$200 \leq \text{EIC} < 750$	$2 \leq \text{SAR} < 3$	$2 \leq \text{Na} < 3$	$1 \leq \text{Cl} < 4$	$1 \leq \text{HCO}_3 < 1.5$

Herein, V_{xy} signifies the recorded values of the parameters, V_{low} denotes the reference value for the lower bounds of the categories, GWQ_{rg} corresponds to the intervals of the categories, and V_{rg} encompasses the ranges of the categories encompassing the specific parameter.

Ultimately, PW_i is computed according to the subsequent Equation (4):

$$PW_i = \frac{\sum_{y=1}^z E_y P_{xy}}{\sum_{y=1}^z \sum_{x=1}^n E_y P_{xy}} \quad (4)$$

In this context, E represents the inherent recording of element y , while P stands as the predominant constraint for parameter x influenced by factor y . Here, x denotes the count of chosen physical and geochemical elements ($1 \leq x \leq n$), and j signifies the count of chosen variables ($1 \leq y \leq z$). xy [43,44].

3.2.2. Sodium Adsorption Ratio Index (SARIndex)

Within the context of irrigating groundwater, the Sodium Adsorption Ratio Index (SARIndex) pertains to the capacity of the soil structure to liberate Ca^{2+} and Mg^{2+} ions while absorbing Na^+ ions at ion exchange sites. This phenomenon disperses soil particles, diminishing their infiltration capacity. Elevated saline water can potentially enhance soil structure by expediting infiltration; however, this can amplify water stress for plants. Consequently, if irrigation water boasts high salinity, plants and crops must exert additional energy to draw moisture out of the soil, leading to a dehydration pressure scenario.

The computation of the SARIndex is executed based on the subsequent Equation (5):

$$\text{SARIndex} = \left(\frac{\text{Na}^+}{\sqrt{\frac{(\text{Ca}^{2+} + \text{Mg}^{2+})}{2}}} \right) \times 100 \text{ (meq/L)} \quad (5)$$

3.2.3. Soluble Sodium Percentage Index (SSPIndex)

The assessment of salinity using the Soluble Sodium Percentage Index (SSPIndex) involves an analysis of the differences between the amounts of Na^{2+} and the proportions of Ca^{2+} and Mg^{2+} . Elevated Na^+ levels relative to calcium and Mg^{2+} can lead to the presence of detrimental agents, contributing to leaf deterioration and the demise of plant tissues.

The computation of the SARIndex is performed according to the subsequent Equation (6):

$$\text{SSPIndex} = \frac{\text{Na}^+}{(\text{Ca}^{2+} + \text{Mg}^{2+} + \text{Na}^+)} \times 100 \text{ (meq/L)} \quad (6)$$

3.2.4. Potential Salinity Index (PSIndex)

Key factors for evaluating groundwater appropriateness for irrigation, as determined by the potential salinity index, include the amount of Cl^- elements and fifty percent of the SO_4^{2-} content. The Potential Salinity Index (PSIndex) is typically categorized into two groups: suspicious if it surpasses three (>5), favorable (3–5), and excellent (<3) for the intention of irrigating crops.

The PSIndex is determined through the subsequent Equation (7):

$$PSIndex = Cl^- + \left(\frac{SO_4^{2-}}{2} \right) (\text{meq/L}) \quad (7)$$

3.2.5. Kelley Index (KIndex)

The calculation of the Kelley Index (KIndex) is executed to assess the appropriateness of groundwater for the purpose of watering crops, revealing an excessive presence of Na^+ within the groundwater composition.

The KIndex computation follows the formulation outlined in Equation (8):

$$KIndex = \frac{\text{Na}^+}{(\text{Ca}^{2+} + \text{Mg}^{2+})} (\text{meq/L}) \quad (8)$$

3.2.6. Residual Sodium Carbonate Index (RSCIndex)

It is frequently employed to ascertain the suitability of irrigation water by comparing elevated levels of CO_3^{2-} and HCO_3^- concentrations in correlation with Ca^{2+} and Mg^{2+} elements. The precipitation of alkali metals, particularly Ca^{2+} and Mg^{2+} , can adversely impact the quality of groundwater used for agricultural watering purposes. Such precipitations, manifesting as carbonate minerals, can elevate the concentration of sodium ions (Na^+) and consequently escalate SARIndex values. High values of Residual Sodium Carbonate (RSCIndex) may detrimentally affect soil physical attributes, contributing to the disintegration of organic matter. This, in turn, can lead to the emergence of discolored marks on the ground once it becomes dry. The Residual Sodium Carbonate Index (RSCIndex) is computed to anticipate the likelihood of Ca^{2+} and Mg^{2+} precipitating at the granules comprising the soil cover, along with the subsequent extraction of the solvent from the land. Notably, elevated RSCIndex levels within groundwater exhibit traits commonly associated with dry and semi-dry regions, resulting in soil characteristics becoming saline and sodic.

The RSCIndex computation is conducted according to the formulation outlined in Equation (9) [43,44]:

$$RSCIndex = (\text{HCO}_3^- + \text{CO}_3^-) - (\text{Ca}^{2+} + \text{Mg}^{2+}) (\text{meq/L}) \quad (9)$$

4. Machine Learning Simulation Models

4.1. Least-Squares Support Vector Machines (LS-SVM) Model

The well-established Machine Learning technique known as Least-Squares Support Vector Machines (LS-SVM) operates on the principles of mathematical learning theory. This approach proves valuable in handling extensive datasets, discerning salient features, and executing regression analyses [45]. Given a set of datasets (x, y) , the primary objective of LS-SVM is to establish functional relationships wherein x constitutes the inlet variable and y constitutes the outlet variable pertaining to the IIGWQIs.

The regressive formulation of the LS-SVM equation is depicted in Equation (10):

$$f(x) = \lambda^t \mu(x) + b \quad (10)$$

Here, the LS-SVM output, denoted as $f(x)$, is governed by a nonlinear mapping function represented by $\mu(x)$. The fine-tuning of the weighting array λ and the bias factor b is achieved through the utilization of the ensuing regularized functions (11):

$$\left\{ \begin{array}{l} \min REG(\lambda, \delta, \delta^*, \varphi) = \frac{1}{2} \Lambda^2 + A[\nu \varphi + \frac{1}{l} \sum_{i=1}^l (\delta_i + \delta_i^*)] \\ \text{subject to } :: y_i - \Lambda^t \mu(x_i) - b \leq \varphi + \delta_i \\ \quad \Lambda^t \mu(x_i) + b - y_i \leq \varphi + \delta_i \\ \quad \delta_i, \varphi \geq 0 \end{array} \right. \quad (11)$$

Here, A signifies the corrective parameter for ensuring stability and the normalization aspect $\|\Lambda\|^2$. The positive slack variables δ_i and δ_i^* come into play. Derived from Lagrange multipliers, the configuration of the LS-SVM model is delineated by the expression (12):

$$\left\{ \begin{array}{l} \text{maxREG}(r_i, r_i^*) = \sum_{i=1}^l (r_i^* - r_i) - \frac{1}{2} \sum_{i=1}^l \sum_{j=1}^l (r_i - r_j^*) (\theta_j - \theta_j^*) \Psi(k_i, k_j) \\ \text{subjective to : } \sum_{i=1}^l (r_i - r_i^*) = 0 \\ 0 \leq r_i, r_i^* \leq \frac{A}{x} \\ \sum_{i=1}^l (r_i + r_i^*) \leq A.v \end{array} \right. \quad (12)$$

In this instance, the kernel function takes the form of $\Psi(k_i, k_j)$, as well as the affirmative Lagrange multipliers, which are symbolized as r_i and r_i^* , respectively.

Upon achieving the target result for the optimization function, the parameters of the LS-SVM are ultimately determined. As a result, the subsequent regressive equation is employed to depict an inlet vector k (13).

$$f(x) = \sum_{i=1}^l (r_i^* - r_i) \Psi(k_i, k_j) + b \quad (13)$$

4.2. Pearson Correlation Fuzzy Inference-Based System (PC-FIS)

The Pearson correlation Fuzzy Inference-based System (PC-FIS) amalgamates the strengths of the Fuzzy Inference System with those of Artificial Intelligence models [46]. The PC-FIS model is conceptualized through diverse inlet-outlet datasets, and the iterative artificial learning framework is later employed to refine the conditions for membership in the model. In this study, the connections between the IIGWQIs and the characteristics of groundwater quality are established through the PC-FIS approaches, and these associations were structured as fuzzy frameworks in the format of if-then statements. The PC-FIS frameworks utilized an interval properties-type FIS for intake membership equations, comprising six equations for the nine intake parameters, while the results were characterized by analog membership functions.

The rule architecture for the interval properties-type model within the PC-FIS is represented as follows (14) and (15):

$$\text{If } \varepsilon = E_1 \text{ and } \zeta = F_1 \text{ we have } \varphi_1 = m_1 \times \varepsilon + n_1 \times \zeta + p_1 \quad (14)$$

$$\text{While, if } \varepsilon = E_2 \text{ and } \zeta = F_2 \text{ we have } \varphi_2 = m_2 \times \varepsilon + n_2 \times \zeta + p_2 \quad (15)$$

In the context of the PC-FIS framework, E and F represent the different scales of magnitude of membership, while ε and ζ signify the function of indirectly ascertaining. The variables m , n , and p correspond to specific constraints that are adjusted during the forward pass of the training algorithm, and φ denotes the result situated within the area marked by irregularities established by the Fuzzy Inference (FIS) theory. The PC-FIS model is composed of five layers, encompassing the membership characteristics of the fuzzy groups E and F , denoted as λE_i and λF_i , respectively [46].

4.3. Assessment of Simulation Model Performance

The predictive abilities of the LS-SVM and PC-FIS models for estimating the IIGWQIs were assessed through the application of the subsequent statistical metrics (16)–(19):

4.3.1. NSE: Nash-Sutcliffe-Efficiency-Coefficient

$$NSE = 1 - \left[\frac{\sum_{i=1}^n (IGWQ_{mi} - IGWQ_{pi})^2}{\sum_{i=1}^n (IGWQ_{mi} - IGWQ_m)^2} \right] \quad (16)$$

4.3.2. MAD: Mean-Absolute-Error

$$MAD = \frac{\sum_{i=1}^n |IGWQ_{mi} - IGWQ_{pi}|}{n} \quad (17)$$

4.3.3. R²: Absolute-Variance-Fraction

$$R^2 = 1 - \frac{\sum_{i=1}^n (IGWQ_{mi} - IGWQ_{pi})^2}{\sum_{i=1}^n (IGWQ_{mi})^2} \quad (18)$$

4.3.4. RMSE: Root-Mean-Square-Error

$$RMSE = \sqrt{\frac{\sum_{i=1}^n (IGWQ_{mi} - IGWQ_{pi})^2}{n}} \quad (19)$$

In this context, “*n*” represents the total count of data observations, where $IGWQ_m$ denotes the measured data, $IGWQ_p$ stands for the predicted data, and $IGWQ$ signifies the mean values of the dataset.

In this study, Electrical Conductivity (ElC), Potassium (K^+), Sodium (Na^+), Calcium (Ca^{2+}), Magnesium (Mg^{2+}), Chloride (Cl^-), Sulfate (SO_4^{2-}), and Bicarbonate (HCO_3^-) were identified as the most significant variables to predict the IIGWQIs. The model structure employed in the Machine Learning algorithms is illustrated in Figure 4.

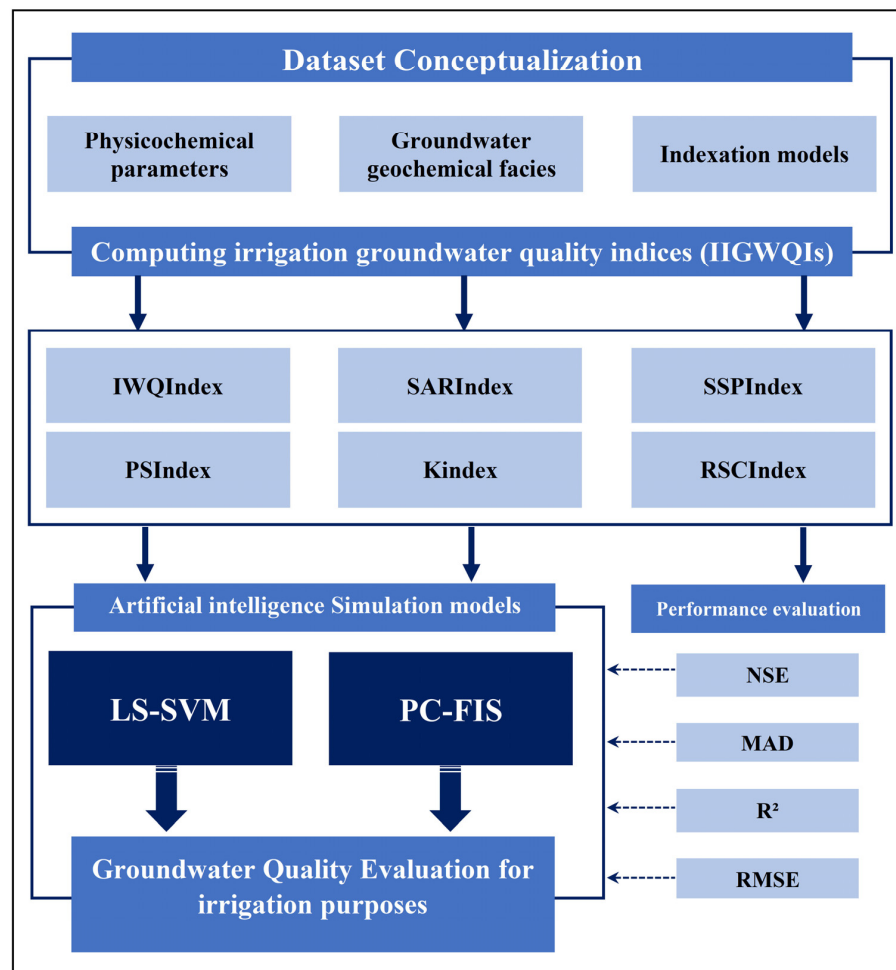


Figure 4. Flowchart of the proposed methodology for IIGWQs.

5. Results and Discussions

5.1. Groundwater Physicochemical Attributes

The following categorization of groundwater was conducted utilizing physicochemical parameters deemed appropriate for irrigation purposes within the Meknassy basin. These parameters are temperature ($T^{\circ}\text{C}$), pH, electrical conductivity (EIC), TDS, potassium, K^+ , Na^+ , Mg^{2+} , Ca^{2+} , Cl^- , SO_4^{2-} , and HCO_3^- , all of which exert an influence on soil quality and agricultural productivity. The geostatistical characteristics of these physicochemical parameters for the 53 groundwater samples are detailed in Table 2.

Table 2. The statistical attributes related to the physicochemical parameters in the analyzed groundwater samples.

	TDS (mg/L)	T° ($^{\circ}\text{C}$)	pH	Ca (mg/L)	Mg (mg/L)	Na (mg/L)	K (mg/L)	HCO_3 (mg/L)	Cl (mg/L)	SO_4 (mg/L)	EIC ($\mu\text{s}/\text{cm}$)
Meknassy Basin (53 Samples)											
Min.	1398	18.7	7.50	116.00	83.00	128.00	10.00	137.00	169.00	475.00	978.60
Max.	4469	39.8	8.30	578.00	371.00	877.00	33.00	723.00	909.00	2284.00	3128.30
Mean	2399.4	24.2	7.92	239.62	145.04	305.94	17.74	232.70	399.92	1058.43	1679.58
Standard Deviation	826.92	4.36	0.19	105.91	58.32	176.30	6.24	92.40	182.27	444.70	578.84

The application of geostatistical investigation shows that the groundwater quality parameters were assessed to determine their maximum and minimum values. The highest recorded electrical conductivity (EIC) value reached $3128.30\text{ }\mu\text{s}/\text{cm}$, while the maximum total dissolved solids (TDS) value observed was 4469 mg/L . The groundwater quality across the Meknassy basin varies between freshwater and brackish. pH levels varied between 7.50 and 8.30, falling within the permissible limits outlined by irrigation water standards. Calcium concentrations were consistent with irrigation water criteria, varying between 116.00 and 578.00 mg/L. Around 11.32% of samples exhibited elevated Mg^{2+} concentrations, surpassing acceptable irrigation thresholds, while the remaining samples demonstrated a mean concentration of 154.04 mg/L . Potassium (K^+) concentrations exceeded allowable irrigation standards across all locations, with values ranging from 10 mg/L to 33 mg/L .

The sodium concentration of the analyzed groundwater samplings displayed a range from moderate to elevated levels, spanning between 128 and 877 mg/L . Among the anions present, Cl^- (ranging from 169 to 909 mg/L) and SO_4^{2-} (ranging from 475 to 2284 mg/L) were the most prevalent. Fortunately, their concentrations remained within acceptable limits for irrigation purposes. Across all water samples, HCO_3^- concentrations fell within the bounds suitable for irrigation water, with the highest recorded concentration reaching 723 mg/L .

5.2. Hydrogeochemical Facies

To classify the groundwater hydrogeochemical facies, a Piper graph was constructed (Figure 5a). The cationic triangle representation revealed that about 61.39% of the entire groundwater samplings exhibited dominance of sodium and potassium, about 32.42% displayed non-dominance, and the remaining samples (6.19%) were dominant in Mg^{2+} . Based on the Piper diagram presentation (Figure 5a), the groundwater samples were categorized into three distinct hydrogeochemical facies. Predominantly, the Ca-Mg-SO₄ facies type (calcium magnesium sulfate facies type) with a characteristic permanent hardness was observed in most samples. The remaining samples were attributed to the mixed Ca-Mg-Cl-SO₄ (mixed facies type) and Na-Cl facies types (sodium chloride facies type). A notable trend among the selected samples was the higher salinity indices ($\text{SO}_4^{2-} + \text{Cl}^-$) compared to alkalinity ($\text{HCO}_3^- + \text{CO}_3^{2-}$), with alkalis ($\text{Na}^+ + \text{K}^+$) slightly outweighing alkaline earths ($\text{Ca}^{2+} + \text{Mg}^{2+}$), thereby serving as a governing factor in shaping the hydrogeochemistry of the Meknassy basin in this region.

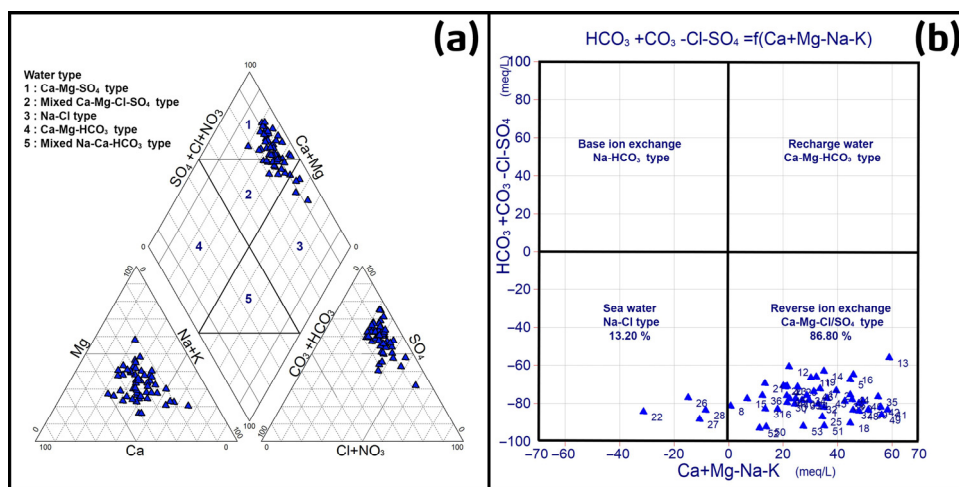


Figure 5. Groundwater hydrogeochemical facies in the Meknassy basin: (a) Piper graph and (b) Chadha diagram.

The predominant geochemical processes governing water chemistry were further validated through the utilization of the Chadha diagram (a modified Piper diagram), as illustrated in Figure 5b. As depicted by the Chadha diagram, a significant portion of the groundwater samplings are situated within the inverse ionic substitution group (Ca-Mg-Cl/SO₄), signifying transitional phases of water development, especially in the north and center parts of the Meknassy basin. Conversely, the remaining samples aligned with the Na-Cl type, suggesting that halite mineral dissolution plays a substantial role in the groundwater chemistry. It is important to emphasize that the progression of groundwater property and suitability for agricultural watering purposes is intricately linked to the prevailing control mechanisms and geochemical processes. Notably, the geochemical attributes of the examined groundwater samplings displayed minimal representation of Ca-Mg-HCO₃ as well as Na-HCO₃ groundwater types, indicating the absence of meteoric or initial water stages within recharge areas. Furthermore, a majority of the samples exhibited characteristics of the Na-Cl groundwater type, signifying the concluding phase of hydrogeochemical development within drainage regions, notably pronounced for the eastern sectors within the Meknassy basin, aligned with the direction of groundwater flow. These outcomes provide corroboration for earlier research in the study vicinity, wherein geochemical modeling was employed to discern the mineralogical saturation condition.

The Durov diagram offers a means to illustrate three key mechanisms: ionic substitution, mixture/dissolving, and inverse ionic substitution, as depicted in Figure 6. Predominantly, the water samples were positioned within the mixture/dissolving group, whereas the remaining subset resided inside the ionic substitution group, thereby reinforcing the earlier elucidation based on statistical analysis.

The application of geostatistical investigation was harnessed to demonstrate the fundamental mechanisms controlling groundwater hydrochemistry within the study area, employing correlations and ratios among different major ions, as depicted in Figure 7. By investigating the connection between EIC and the Sodium/Calcium proportion, insights into the impact of the dissolving and evaporating processes within the Meknassy basin were garnered. The Na⁺/Cl⁻ ratio exhibited a nearly constant trendline as EIC increased, a phenomenon attributed to NaCl dissolving. Additionally, the samples positioned above and below the 1:1 line indicated instances of direct ionic substitution and inverse ionic substitution, respectively (Figure 7a). To further substantiate the significance of dissolving, direct ionic substitution, and inverse ionic substitution as pivotal characteristics influencing the water hydrogeochemistry of the Meknassy basin, a series of ion-graphs and a Chadha plot were employed.

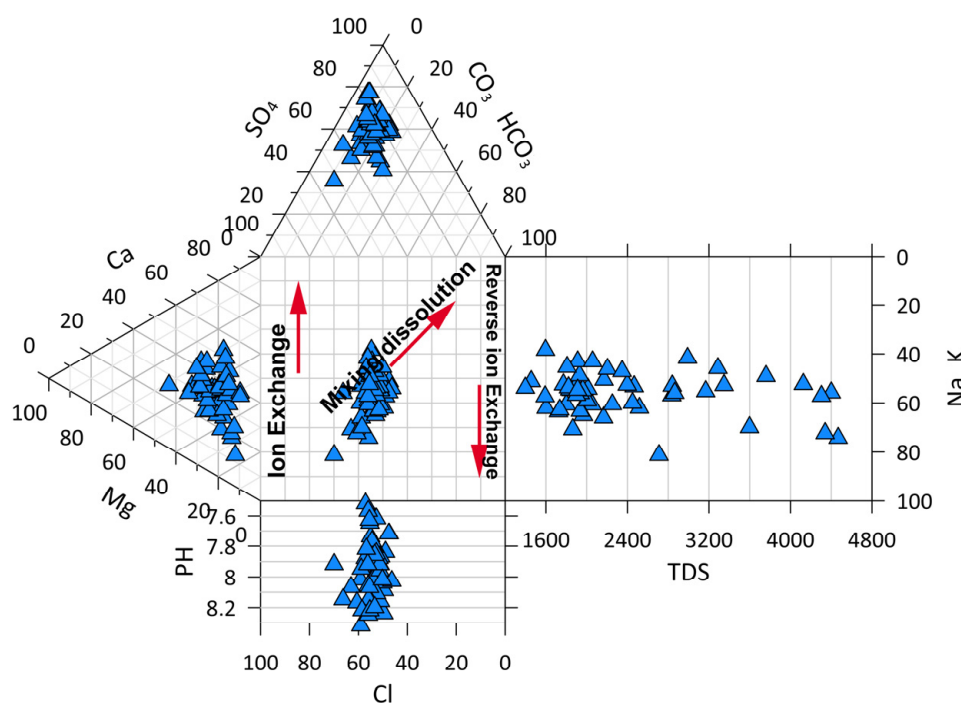


Figure 6. Durov diagram showing the key mechanisms controlling groundwater geochemistry.

The analogue associations between sodium and calcium highlight a subtle equilibrium between these two ions, and a notable proportion of the groundwater sampling closely aligns with the 1:1 line graph, possibly due to a shared origin, like NaCl dissolving (Figure 7b). The effects of NaCl dissolving, especially within the non-saturated area, are a distinctive feature of dry and partially dry regions. Water samples positioned below the 1:1 line graph could suggest an augmentation in Cl^- levels originating from an extra origin of Cl^- ions or a potential reduction in sodium levels because of Na^+ removal from the groundwater. Excessive use of groundwater for irrigation crops and improper waste disposal are both considered human-related actions that could potentially contribute to the elevated levels of chloride. In certain samples, the Na^+/Cl^- ratio exceeded 1, suggesting a direct ion exchange process. The correlation between $\text{Na}^+ + \text{K}^+$ and $\text{Ca}^{2+} + \text{Mg}^{2+}$ (depicted in Figure 7c) demonstrated that a substantial portion of water samples aligned closely with the 1:1 line, implying mineralogical dissolving, while a smaller number of samples deviated higher than the line due to inverse ionic substitution phenomena. The prevalence of Ca^{2+} and Mg^{2+} over Na^+ and K^+ in most groundwater samples signifies that the ionic substitution operation and carbonate dissolution led to the replacement of sodium and potassium ions with calcium and magnesium ions (Table 3). A few groundwater samples exceeded the 1:1 line, showing the presence of inverse ionic substitution. This observation was drawn from a linear graph (depicted in Figure 7d) depicting the cumulative sum of calcium and magnesium ions facing the total of bicarbonates and sulfate ions. The crossing of the 1:1 line was attributed to the breakdown of carbonates (CaCO_3 and $\text{CaMg}(\text{CO}_3)_2$). The relative augmentation of $\text{Ca}^{2+} + \text{Mg}^{2+}$ ions in comparison to $\text{SO}_4^{2-} + \text{HCO}_3^-$ ions was a result of carbonate weathering.

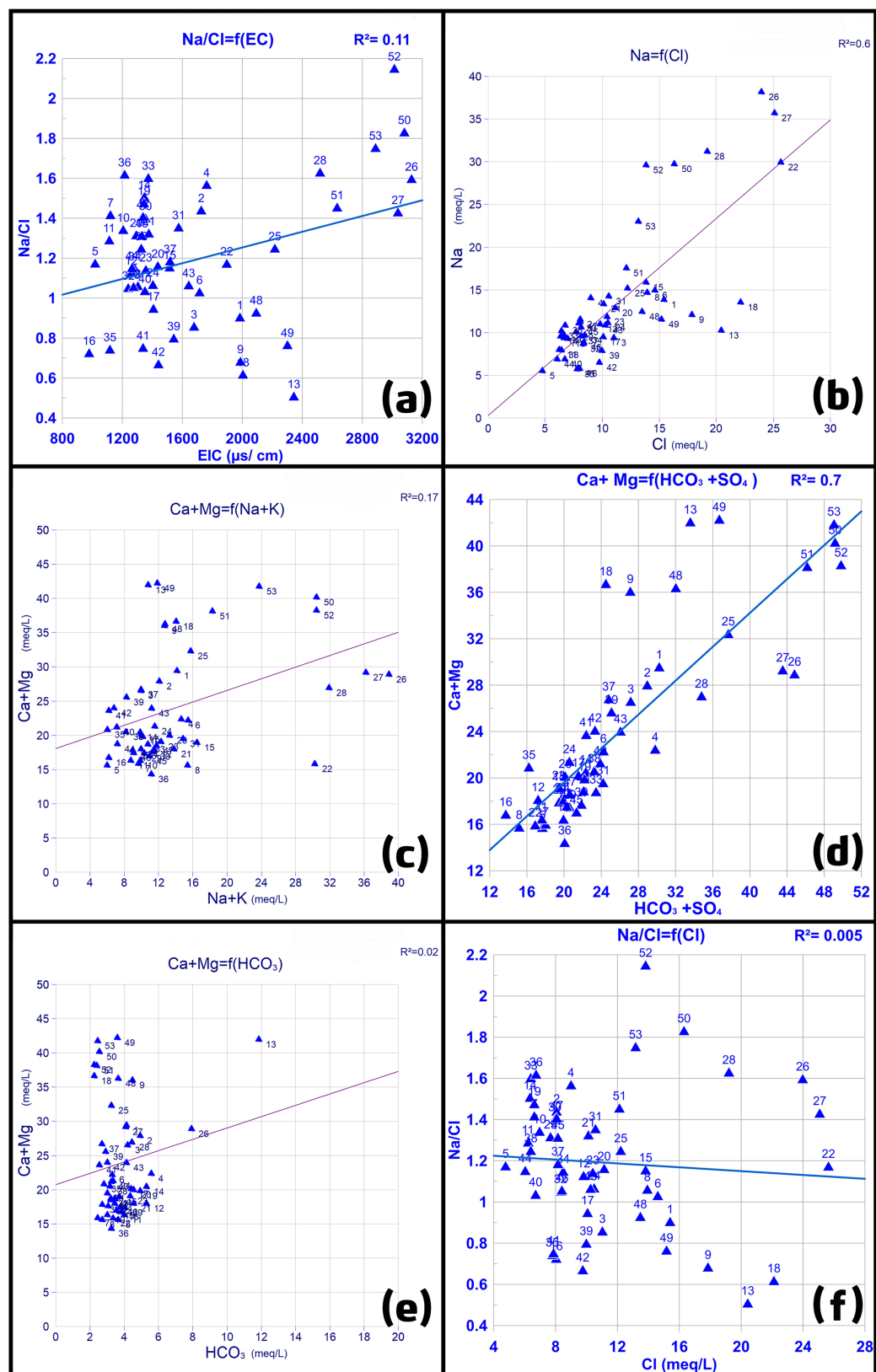


Figure 7. Correlations and ratios among different major ions: (a) Na/Cl and EC ; (b) Na and Cl ; (c) $\text{Ca} + \text{Mg}$ and $\text{Na} + \text{K}$; (d) $\text{Ca} + \text{Mg}$ and $\text{SO}_4^{2-} + \text{HCO}_3^{-}$; (e) $\text{Ca} + \text{Mg}$ and HCO_3^{-} ; (f) Na/Cl and Cl .

Table 3. Correlation matrix of chemical elements in groundwater from the fractured aquifer of the Meknassy basin.

	TDS	T°	pH	EIC	Ca	Mg	Na	K	HCO ₃	Cl	SO ₄
TDS	1										
T°	0.28	1									
pH	-0.03	-0.63	1								
EIC	0.99	0.21	0.02	1							
Ca	0.78	0.69	-0.30	0.7	1						
Mg	0.53	-0.15	0.28	0.5	0.28	1					
Na	0.83	0.08	0.00	0.9	0.48	0.16	1				
K	0.60	0.09	0.04	0.6	0.42	0.27	0.57	1			
HCO ₃	0.17	-0.49	0.30	0.2	-0.16	0.44	0.1	0.14	1		
Cl	0.75	-0.16	0.26	0.8	0.32	0.57	0.77	0.41	0.29	1	
SO ₄	0.92	0.52	-0.19	0.9	0.89	0.4	0.68	0.53	-0.07	0.46	1

The $\text{Ca}^{2+} + \text{Mg}^{2+}$ to HCO_3^- ratio offers insight into the origin of Ca^{2+} and Mg^{2+} within the samplings (as depicted in Figure 7e). A substantial majority of the groundwater samplings exhibited a notably higher $\text{Ca}^{2+} + \text{Mg}^{2+}/\text{HCO}_3^-$ ratio, indicative of carbonate and silicate mineral weathering contributing to the presence of $\text{Ca}^{2+} + \text{Mg}^{2+}$. Thus, the elevated levels of Ca^{2+} and Mg^{2+} cannot be solely attributed to carbonate dissolution (calcite and dolomite), suggesting the involvement of diverse hydrogeochemical processes. The $\text{Ca}^{2+} + \text{Mg}^{2+}/\text{HCO}_3^-$ ratio holds significance in identifying the meteoric nature and fresh groundwater recharge. A ratio below 1 signifies meteoric water and the presence of groundwater recharge. Within the Meknassy basin, the majority (92%) of the samples exceeded a value of 1, implying minimal meteoric processes and groundwater recharge.

The correlation from Na^+/Cl^- to Cl^- (as shown in Figure 7f) exposes a reverse relationship, indicating that the argillaceous materials within the aquifer contain the argil substitute Na^+ , liberated during salt disintegration, with Ca^{2+} and Mg^{2+} (Table 3).

5.3. Integrated Irrigation Groundwater Quality Indices (IIGWQIs) for Agricultural Implication

Given the intricate interplay of farming methods, soil attributes, and the quality of groundwater, a range of indices have been applied within this research endeavor to evaluate the appropriateness of groundwater for the purpose of irrigating crops. The employed indices encompass the Irrigation Water Quality Index (IWQIndex), Kelley Index (KIndex), Sodium Adsorption Ratio Index (SARIndex), Soluble Sodium Percentage Index (SSPIndex), Potential Salinity Index (PSIndex), and Residual Sodium Carbonate Index (RSCIndex). Through these methodologies, the potential for soil salinization is elucidated, shedding light on the adverse impact of watering on soil and plant well-being. Employing statistical analyses, the data derived from the IIGWQIs underwent rigorous evaluation to assess the appropriateness of groundwater for agricultural use (Tables 4 and 5).

Table 4. The statistical properties of various IIGWQIs.

	IWQIndex	SARIndex	SSPIndex	PSIndex	KIndex	RSCIndex
Min.	29.73	0.19	3.87	-0.78	0.11	-9.89
Max.	99.62	8.37	66.46	12.18	2.05	2.68
Mean	80.46	3.12	48.61	3.48	1.10	-2.32
Standard Deviation	22.90	2.05	10.47	3.21	0.48	2.52

Table 5. Categorization of the IIGWQIs groups for irrigation use.

IIGWQIs	Class	Water Category	Number of Samples	Percentage of Samples (%)
IWQIndex	0–40	Extreme limitation	8	15.09
	40–55	Severe limitation	3	5.66
	55–70	Moderate limitation	1	1.89
	70–85	Minimal limitation	6	11.32
	85–100	No limitation	35	66.04
SARIndex	>26	Unfavorable	29	54.72
	18–26	Suspicious	16	30.19
	10–18	Favorable	8	15.09
	<10	Excellent	0	0.00
SSPIndex	>60	Insecure	4	7.55
	<60	Secure	49	92.45
PSIndex	>5	Suspicious	18	33.96
	3–5	Favorable	24	45.28
	<3	Excellent	11	20.76
KIndex	>1	Unfavorable	10	18.87
	<1	Favorable	43	81.13
RSCIndex	>2.5	Insecure	6	11.32
	1.25–2.5	Average	37	69.81
	<1.25	Secure	10	18.87

5.3.1. IWQIndex: Irrigation Water Quality Index

The range of IWQIndex values fell between 29.73 and 99.62, averaging 80.46 (as depicted in Table 4). Analyzing the IWQIndex values in the context of the Meknassy basin, a significant portion of the samples (about 66.04%) were categorized within the “no limitation” class, suitable for crops with salt tolerance. Approximately 13.21% of the groundwater sampling lay within the spectrum of “minimal to moderate limitation”, while roughly 20.75% were categorized as experiencing “severe to extreme limitation” for irrigation purposes. This latter category can be employed for irrigating crops that exhibit moderate to severe sensitivity to salt, especially when cultivated within unconsolidated soil devoid of compressed strata (as outlined in Table 5).

The comprehensive IIGWQIs geospatial maps (depicted in Figure 8a) serve as a valuable tool in assessing the appropriateness of groundwater for agricultural watering, offering insights into the adequacy of groundwater based on physical and chemical parameters. Analyzing the IWQIndex values, it becomes evident that the water quality experiences a decline in the northern and eastern sectors of the Meknassy region, primarily attributed to anthropogenic activities and geological influences.

5.3.2. SARIndex: Sodium Adsorption Ratio Index

The USSL diagram offers a visual representation of the relationship between the Sodium Adsorption Ratio (SARIndex) and Electrical Conductivity, as depicted in Figure 9. Most of the collected groundwater samples predominantly occupied the regions between C3-S1 and C4-S2 (characterized by low SARIndex and medium to high salinity levels). Among these, 43 samples were classified under the C3-S1 category, signifying high salinity and low SARIndex. Additionally, five samples from the Meknassy basin were situated within the C4-S2 classification, denoting elevated levels of salinity and moderate SARIndex values. A smaller subset, comprising only two samples, fell within the C4-S3 category, indicative of high salinity and high SARIndex values. Notably, the SARIndex values for all investigated samples remained below 10, suggesting an excellent classification for irrigation suitability, as illustrated in Figure 8b.

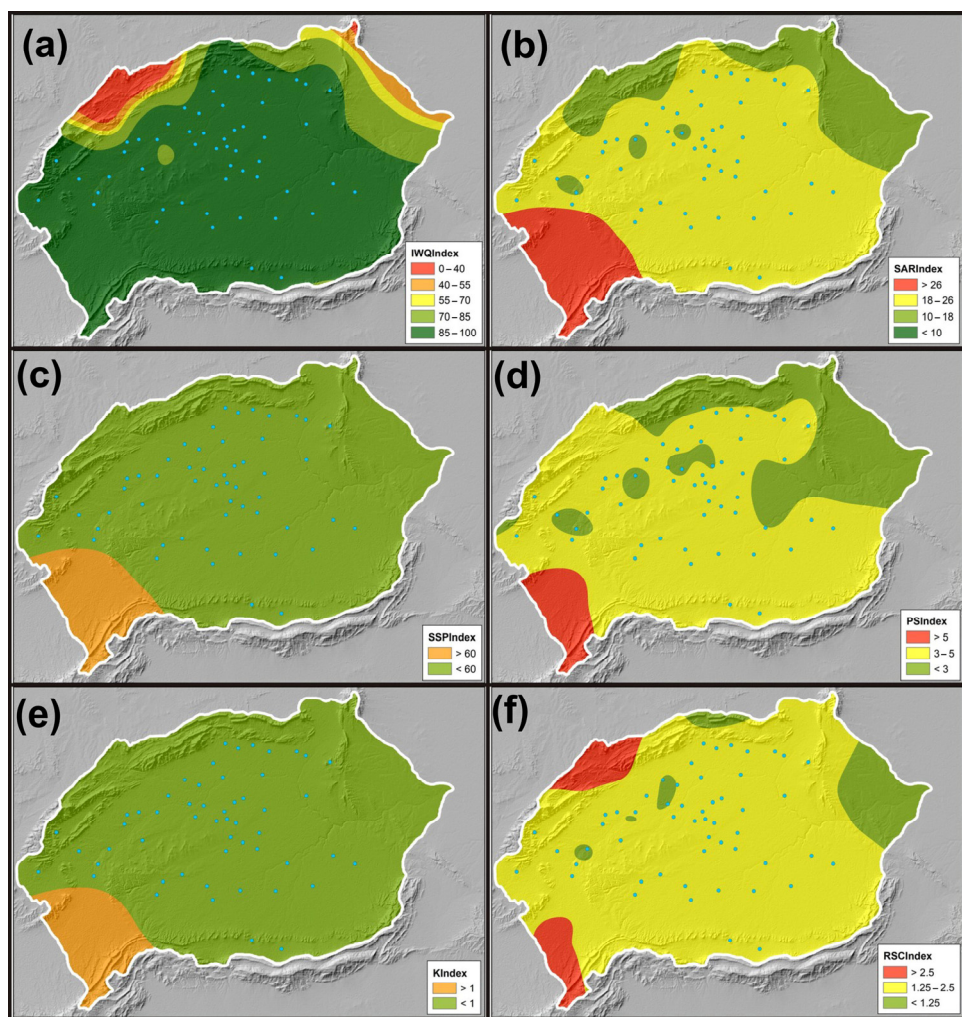


Figure 8. Comprehensive IIWQI geospatial maps of the Meknassy basin: (a) IWQIndex, (b) SARIndex, (c) SSPIIndex, (d) PSIndex, (e) KIndex, and (f) RSCIndex.

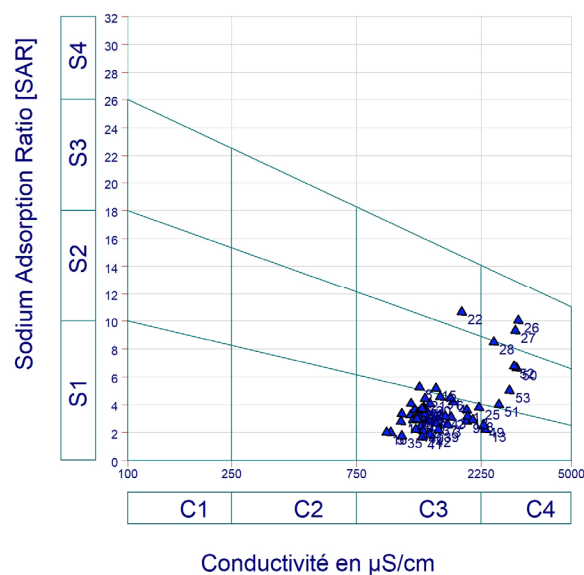


Figure 9. USSL diagram for irrigation purposes.

The findings indicate that elevated salinity levels in irrigation water can have detrimental effects on plant growth. However, the soil infiltration capacity remains unaffected by low to medium SARIndex values (as shown in Figure 9) and the absence of calcium-related conditions. To effectively manage groundwater utilization for irrigation in areas experiencing degradation, a recommended strategy is the selection of plant varieties that demonstrate resilience to the elevated salinity of the water.

5.3.3. SSPIndex: Soluble Sodium Percentage Index

The soluble sodium percentage index (SSPIndex) exhibited a spectrum of values spanning from 3.87 to 66.46, with an average of 48.61. The analysis of SSPIndex outcomes indicated that most of the collected water samples, totaling 92.45%, are classified within the secure category suitable for irrigation purposes. In contrast, a smaller subset, constituting 7.55% of the samples, fell into the unsafe category, as depicted in Figure 8c.

5.3.4. PSIndex: Potential Salinity Index

The potential salinity index (PSIndex) exhibited a diverse range, spanning from -0.78 to 12.18, with an average value of 3.48. The assessment of PSIndex values categorized 66.04% of the samples (35 samples) as belonging to the favorable to excellent range. In contrast, the remaining subset of samples, totaling 18 samples (33.96%), were classified within the suspicious class, as visually illustrated in Figure 8d.

5.3.5. KIndex: Kelley Index

The KIndex values exhibited a range of variability spanning from 0.11 to 2.05, with an average value of 1.10. The analysis of KIndex outcomes delineates that a significant portion of the groundwater samples, specifically 81.13% (comprising 43 samples), were classified as favorable for irrigation purposes. In contrast, the remaining subset of samples (constituting 10 samples—18.87%) received a categorization of unfavorable (as shown in Table 2).

The interpretation of KIndex results is guided by a threshold of one, where each KIndex record exceeding this threshold ($KIndex > 1$) signifies an elevated presence of Na^+ within the groundwater. Conversely, each KIndex record below 1 ($KIndex < 1$) signifies the water's suitability for watering purposes. The distribution of unsuitable water samples is predominantly observed in the southwestern regions of the Meknassy basin, as visually depicted in Figure 8e.

5.3.6. RSCIndex: Residual Sodium Carbonate Index

Based on the RSCIndex records, the groundwater is categorized into three distinct categories. Groundwater designated for watering purposes is considered acceptable when its RSCIndex falls below 1.25 or between 1.25 and 2.5. However, water surpassing an RSCIndex of 2.5 is deemed unsuitable. In the context of this study, 10 water samples (18.87%) exhibited an RSCIndex value below 1.25, signifying their suitability for watering purposes and assurance of meeting high standards of safety and quality. Meanwhile, 37 samples (69.81%) resided within the moderate class, while the rest of the samples (6 samples—11.32%) were classified as falling below the acceptable threshold (Figure 8f).

The outcomes derived from the IIGWQIs indicate a gradual decline in groundwater quality across the expanse of the Meknassy basin, extending from its eastern to western regions. This trend has the potential to induce sodification, impair the physical attributes of the soil, lead to carbon-based natural substance dissociation, and promote salt accumulation in the soil. In the context of effective groundwater resource management within the western sector of the Meknassy basin, the optimal approach involves the application of calcium-based fertilizers to counteract potential sodification effects. Additionally, cultivating plant varieties with higher salt tolerance can prove beneficial in mitigating the impact of increased salinity. Furthermore, groundwater sourced from the western area of the Meknassy basin can be suitably utilized for irrigating crops characterized by medium

to elevated susceptibility to salinity, particularly for unconsolidated soil without densely packed strata.

Assessment of land assets and categorization of soil reveals a distribution of soils categorized as adequate, subpar, and extremely deficient based on considerations of salinity, alkalinity, and soil texture. These classifications align with findings from prior studies [37,38], reinforcing the identified characteristics of the soil.

5.4. Models' Simulation

5.4.1. LS-SVM Model

Python was utilized for coding both the LS-SVM and PC-FIS models. For IIGWQI prediction, Pytorch-SciPy packages and algorithms were implemented. In order to achieve precise forecasting capabilities concerning the LS-SVM simulation framework, the optimized shuffled complex evolution algorithm (SCE-UA) was employed via SpotPy (Statistical Parameter Optimization Tool for Python). After choosing the most effective LS-SVM simulation framework during the learning phase, calculations were made for the expected values of the identified IIGWQIs (Figure 10), followed by a comparative analysis of the projected/inspected values. The effectiveness of the model outcomes was displayed within Table 6, incorporating metrics such as NSE, MAD, R^2 , and MRSE. During the IWQIndex training sequences, the performance metrics were as follows: NSE = 0.96, MAD = 0.59, R^2 = 0.96, and RMSE = 1.50; whereas in the testing sequences, they were NSE = 0.68, MAD = 8.43, R^2 = 0.75, and RMSE = 12.38. Notably, a discernible decline in performance is evident when transitioning to the testing phase. Specifically, the LS-SVM model tended to overestimate the predicted IWQIndex values during testing. Turning to the SARIndex, the model's performance measures for the training sequences were NSE = 0.98, MAD = 0.23, R^2 = 0.92, and RMSE = 0.50, whereas for the testing sequences, they were NSE = 0.18, MAD = 1.43, R^2 = 0.35, and RMSE = 2.16. Generally, the LS-SVM model demonstrated diminished performance during the testing period across all indices.

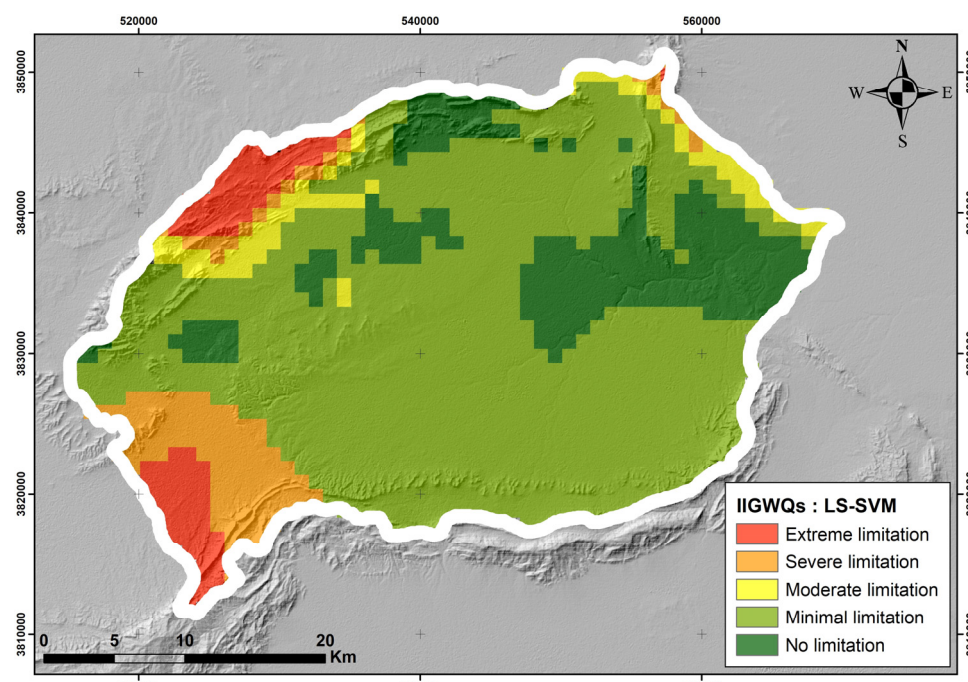


Figure 10. Map of the proposed IIGWS in the Meknassy basin according to the LS-SVM model.

Table 6. Simulation models' performance criteria for predicting IIGWQIs.

IIGWQI Indexes	Simulation Models	Performance Criteria			
		NSE	MAD	R ²	RMSE
Training sequences	IWQIndex	LS-SVM	0.96	0.59	0.96
		PC-FIS	0.97	1.83	0.98
	SARIndex	LS-SVM	0.89	0.23	0.92
		PC-FIS	0.93	0.14	0.94
	SSPIndex	LS-SVM	0.15	7.01	0.67
		PC-FIS	0.68	4.00	0.69
	PSIndex	LS-SVM	0.95	0.23	0.97
		PC-FIS	0.97	0.02	0.98
	KIndex	LS-SVM	0.24	0.14	0.49
		PC-FIS	0.42	0.08	0.47
	RSCIndex	LS-SVM	0.97	0.00	0.98
		PC-FIS	0.94	0.20	0.95
Testing sequences	IWQIndex	LS-SVM	0.68	8.43	0.75
		PC-FIS	0.94	3.04	0.96
	SARIndex	LS-SVM	0.18	1.43	0.35
		PC-FIS	0.92	0.20	0.93
	SSPIndex	LS-SVM	-0.02	8.85	0.52
		PC-FIS	0.61	4.49	0.67
	PSIndex	LS-SVM	0.57	1.33	0.71
		PC-FIS	0.98	0.03	0.99
	KIndex	LS-SVM	-0.07	0.26	0.48
		PC-FIS	0.66	0.08	0.68
	RSCIndex	LS-SVM	-0.18	1.88	0.60
		PC-FIS	0.96	0.17	0.97

5.4.2. PC-FIS Model

Once the optimal model was identified through PC-FIS training, the anticipated estimates for the Integrated Irrigation Groundwater Quality Indices (IIGWQIs) were calculated (Figure 11). A comparative analysis of the forecasted values for IWQIndex and SARIndex, both within the learning and validation sequences, against the current dataset demonstrated a strong alignment between the two curves. While some values deviated significantly from the recorded data, the general trends of the projected/inspected data sets intimately resembled each other. A remarkable R² value (0.98) underscored the impeccable consensus among the projected/inspected IWQIndex values. The developed PC-FIS simulation framework exhibited exceptional suitability regarding the IIGWQIs for the learning and validation phases (NSE records in Table 6), all exceeding 0.90. Notably, Table 6 illustrates the superiority of the PC-FIS model regarding precision across all indicators, surpassing the effectiveness of the LS-SVM simulation framework. Throughout the transition from learning to validation phases, the PC-FIS model's performance metrics (MAD, R², and RMSE) experienced only marginal fluctuations. A more pronounced distinction becomes apparent when comparing the predicted/observed IIGWQIs in the learning and validation sequences, in addition to the correlative diagrams. The temporal groups' diagrams revealed the PC-FIS simulation framework's proficiency in discerning the fluctuating patterns within the observed IIGWQI data.

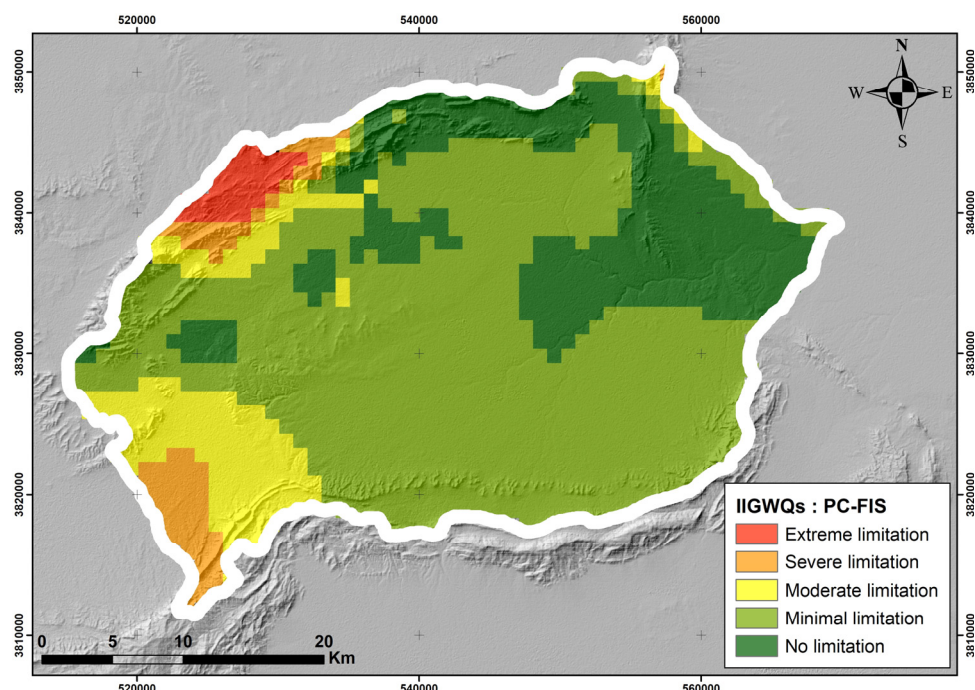


Figure 11. Map of the proposed IIGWS in the Meknassy basin according to the PC-FIS model.

An integral goal of the current research was to evaluate the appropriateness of groundwater for farming purposes through diverse Integrated Irrigation Groundwater Quality Indices (IIGWQIs). Traditionally, the computation of these indices relies on classical mathematical formulas, a process known to be time-intensive, particularly due to the extensive data volume and numerous steps involved in reaching the final outcomes. In response, we introduced the PC-FIS and LS-SVM models, which efficiently handle substantial datasets of nonlinear systems. These models swiftly and accurately discern patterns, make forecasts for IIGWQIs with a commendable level of precision and efficiency, streamline processes, and derive results through simulations. Furthermore, simulation models serve as valuable tools for foreseeing outcomes in scenarios where practical experimentation might be unfeasible or impractical.

The findings substantiate the effectiveness of employing the PC-FIS and LS-SVM models in evaluating and managing groundwater quality for irrigation across the Meknassy basin. Ultimately, the integration of IIGWQIs, along with the application of PC-FIS and LS-SVM, demonstrated itself as a valuable and pragmatic approach for discerning and projecting the quality of groundwater for watering, particularly within dry and semi-dry environments.

5.4.3. The Relevance of Theory and Practice

The possible effects regarding the suggested approach are contingent upon the extent of the investigation and the accessibility of data sets. There is room for its expansion to encompass a broader regional context, thereby providing strategic insights to decision-makers and stakeholders. However, it remains imperative to possess a comprehensive understanding of the pivotal hydrogeological conditions in order to uphold relevance and precision in the outcomes.

The suggested preliminary assessment process can offer substantial advantages to decision-makers and stakeholders by considerably streamlining the time and resources typically allocated to conventional, intricate strategies. By tailoring management approaches to address the specific scenarios highlighted by the study, the derived results stand to gain enhanced value. Ultimately, both the natural environment and the socioeconomic fabric of the region could experience long-term benefits from such an approach.

6. Conclusions

This study employed a combination of physicochemical parameters, Integrated Irrigation Groundwater Quality Indices (IIGWQIs), and Geographic Information System (GIS) facilities for the delineation of geochemical types of groundwater as well as the governing procedures. The primary aim was to evaluate the appropriateness of the Meknassy basin's groundwater basin regarding agricultural purposes. The collection of physicochemical data encompassed measurements from 53 groundwater wells. The hydrogeochemical facies identified included Ca-Mg-SO₄, mixed Ca-Mg-Cl-SO₄, and Na-Cl facies, revealing processes such as carbonate weathering, carbonate dissolution, interactions between rocks and groundwater, and mixing ionic substitution.

For instance, IWQIndex, SSPIndex, PSIndex, KIndex, and RSCIndex classifications demonstrated that a majority of collected groundwater samples exhibited suitability for watering purposes with minimal limitations (77.36%), deemed secure (92.45%), rated as favorable to excellent (66.04%), categorized as favorable (81.13%), and indicated average to secure quality (88.68%). However, only 15.09% were rated as favorable, according to SARIndex.

To simulate IIGWQIs, two predictive models were created according to the gathered physical and chemical factors. The proposed evaluation of the simulation models revealed their capability to accurately predict IWQIndex during both the training sequences ($R^2 = 0.96, 0.97$) and testing sequences ($R^2 = 0.68, 0.94$), indicating their potential for IIGWQI prediction. Consequently, the synergistic integration of physicochemical parameters, IIGWQIs, GIS, and Machine Learning models offers a robust approach for efficient groundwater utilization in irrigation.

This research aimed to transcend the limitations of conventional methods by employing PC-FIS and LS-SVM models to predict groundwater quality for the purpose of watering within the scope of substantial salt contamination. The initial outcomes of this endeavor provide valuable insights pertaining to the effective and precise administration of groundwater reserves within the Meknassy area, serving as a foundation for water resource risk mitigation strategies. The methodology proposed herein holds potential for further refinement to enhance accuracy under diverse conditions, empowering decision-makers to employ a combination of technologies for groundwater quality administration and strategic organization.

At the bottom, integrating IIGWQIs, Machine Learning, and GIS methodologies offers an alternative approach to data analysis, yielding prompt results with reduced time investment while achieving satisfactory outcomes in the realm of groundwater quality management.

Author Contributions: Conceptualization, M.H.M.; Methodology, Y.M.; Software, M.H.M.; Validation, L.Z. and I.C.; Formal analysis, M.H.M. and Y.M.; Investigation, I.C. and A.Z.; Resources, I.C. and A.Z.; Data curation, Y.M.; Writing—original draft, M.H.M.; Writing—review & editing, L.Z., I.C. and A.Z.; Visualization, A.Z.; Supervision, L.Z. and I.C.; Project administration, L.Z. and I.C.; Funding acquisition, L.Z. and I.C. All authors have read and agreed to the published version of the manuscript.

Funding: This research was funded by the “Programme de Partenariat Hubert Curien (PHC) franco-tunisien UTIQUE-PHC-Utique France (Institut Polytechnique UniLaSalle Beauvais) et Tunisie (Université de Tunis El Manar)” through the CMCU Tunisian French University Cooperation PHC UTIQUE 2022 (Project Number: 22G1003).

Data Availability Statement: Data are available from the Regional Commissary for Agricultural Development Sidi Bouzid—CRDA Sidi Bouzid (agricultural map).

Acknowledgments: The authors acknowledge funding from the “Programme de Partenariat Hubert Curien (PHC) franco-tunisien UTIQUE-PHC-Utique France (Institut Polytechnique UniLaSalle Beauvais) et Tunisie (Université de Tunis El Manar)” through the CMCU Tunisian French University Cooperation PHC UTIQUE 2022 (Project Number: 22G1003). The authors appreciate the collaboration

between Tunis El Manar University and “AGHYLE, Institut Polytechnique UniLaSalle Beauvais, SFR Condorcet FR CNRS 3417, 19 Rue Pierre Waguet, 60026 Beauvais, France”.

Conflicts of Interest: The authors declare no conflict of interest.

References

1. Velasco-Muñoz, J.F.; Aznar-Sánchez, J.A.; Belmonte-Ureña, L.J.; Román-Sánchez, I.M. Sustainable Water Use in Agriculture: A Review of Worldwide Research. *Sustainability* **2018**, *10*, 1084. [[CrossRef](#)]
2. Mirzaei, A.; Saghabian, B.; Mirchi, A.; Madani, K. The Groundwater—Energy—Food Nexus in Iran’s Agricultural Sector: Implications for Water Security. *Water* **2019**, *11*, 1835. [[CrossRef](#)]
3. Mancosu, N.; Snyder, R.L.; Kyriakakis, G.; Spano, D. Water Scarcity and Future Challenges for Food Production. *Water* **2015**, *7*, 975–992. [[CrossRef](#)]
4. Msaddek, M.H.; Souissi, D.; Moumni, Y.; Chenini, I.; Bouaziz, N.; Dlala, M. Groundwater Potentiality Assessment in an Arid Zone Using a Statistical Approach and Multi-Criteria Evaluation, Southwestern Tunisia. *Geol. Q.* **2019**, *63*, 10. [[CrossRef](#)]
5. Chenini, I.; Zghibi, A.; Msaddek, M.H.; Dlala, M. Groundwater Vulnerability Mapping in Urbanized Hydrological System Using Modified Drastic Model and Sensitivity Analysis. *Environ. Eng. Geosci.* **2018**, *24*, 293–304. [[CrossRef](#)]
6. Ait Lemkademe, A.; El Ghorfi, M.; Zouhri, L.; Hedoun, O.; Khalil, A.; Maacha, L. Origin and Salinization Processes of Groundwater in the Semi-Arid Area of Zagora Graben, Southeast Morocco. *Water* **2023**, *15*, 2172. [[CrossRef](#)]
7. El Amari, K.; Zouhri, L.; Benkaddour, A.; Toughzaoui, S.; Hibti, M.; Essarraj, S. Mineralization of water resources of Roc-Blanc watershed (Morocco) et al. Mineralization of water resources of Roc-Blanc watershed (Morocco). *Environ. Earth Sci.* **2021**, *80*, 479. [[CrossRef](#)]
8. Zouhri, L.; El Amari, K.; Marier, D.; Benkaddour, A.; Hibti, M. Bacteriological and geochemical features of the groundwater resources: Kettara abandoned mine (Morocco). *Environ. Pollut.* **2019**, *252*, 1698–1708. [[CrossRef](#)]
9. Moyé, J.; Picard-Lesteven, T.; Zouhri, L.; El Amari, K.; Hibti, M.; Benkaddour, A. Groundwater assessment and environmental impact in the abandoned mine of Kettara (Morocco). *Environ. Pollut.* **2017**, *231*, 899–907. [[CrossRef](#)]
10. Sebei, A.; Slama, T.; Helali, M.A. Hydrochemical Characterization and Geospatial Analysis of Groundwater Quality in Cap Bon Region, Northeastern Tunisia. *Environ. Earth Sci.* **2018**, *77*, 557. [[CrossRef](#)]
11. Sattari, M.T.; Feizi, H.; Colak, M.S.; Ozturk, A.; Ozturk, F.; Apaydin, H. Surface water quality classification using data mining approaches: Irrigation along the Aladag River. *Irrig. Drain.* **2021**, *70*, 1227–1246. [[CrossRef](#)]
12. Farid, H.U.; Ayub, H.U.; Khan, Z.M.; Ahmad, I.; Anjum, M.N.; Kanwar, R.M.A.; Mubeen, M.; Sakinder, P. Groundwater quality risk assessment using hydro-chemical and geospatial analysis. *Environ. Dev. Sustain.* **2023**, *25*, 8343–8365. [[CrossRef](#)]
13. Giri, A.; Bharti, V.K.; Kalia, S.; Kumar, K.; Khansu, M. Hydrochemical and quality assessment of irrigation water at the trans-himalayan high-altitude regions of Leh, Ladakh, India. *Appl. Water Sci.* **2022**, *12*, 197. [[CrossRef](#)]
14. Laonamsai, J.; Pawana, V.; Chiphamlong, P.; Chomcheawchan, P.; Kamdee, K.; Kimmany, B.; Julphunthong, P. Groundwater Quality Variations in Multiple Aquifers: A Comprehensive Evaluation for Public Health and Agricultural Use. *Geosciences* **2023**, *13*, 195. [[CrossRef](#)]
15. Ibrahim, H.; Yaseen, Z.M.; Scholz, M.; Ali, M.; Gad, M.; Elsayed, S.; Khadr, M.; Hussein, H.; Ibrahim, H.H.; Eid, M.H.; et al. Evaluation and Prediction of Groundwater Quality for Irrigation Using an Integrated Water Quality Indices, Machine Learning Models and GIS Approaches: A Representative Case Study. *Water* **2023**, *15*, 694. [[CrossRef](#)]
16. Tziritis, E.; Sachsamanoglou, E.; Aschonitis, V. Assessing Groundwater Evolution with a Combined Approach of Hydrogeochemical Modelling and Data Analysis: Application to the Rhodope Coastal Aquifer (NE Greece). *Water* **2023**, *15*, 230. [[CrossRef](#)]
17. Wang, Y.; Li, R.; Wu, X.; Yan, Y.; Wei, C.; Luo, M.; Xiao, Y.; Zhang, Y. Evaluation of Groundwater Quality for Drinking and Irrigation Purposes Using GIS-Based IWQI, EWQI and HHR Model. *Water* **2023**, *15*, 2233. [[CrossRef](#)]
18. Li, P.; Wu, J.; Qian, H. Assessment of groundwater quality for irrigation purposes and identification of hydrogeochemical evolution mechanisms in Pengyang County, China. *Environ. Earth Sci.* **2013**, *69*, 2211–2225. [[CrossRef](#)]
19. Asadi, E.; Isazadeh, M.; Samadianfar, S.; Ramli, M.F.; Mosavi, A.; Nabipour, N.; Shamshirband, S.; Hajnal, E.; Chau, K.-W. Groundwater Quality Assessment for Sustainable Drinking and Irrigation. *Sustainability* **2020**, *12*, 177. [[CrossRef](#)]
20. Egbueri, J.C.; Agbasi, J.C. Performances of MLR, RBF-NN, and MLP-NN in the evaluation and prediction of water resources quality for irrigation purposes under two modeling scenarios. *Geocarto Int.* **2022**, *37*, 14399–14431. [[CrossRef](#)]
21. Mukherjee, I.; Singh, U.K.; Chakma, S. Evaluation of groundwater quality for irrigation water supply using multi-criteria decision-making techniques and GIS in an agroeconomic tract of Lower Ganga basin, India. *J. Environ. Manag.* **2022**, *309*, 114691. [[CrossRef](#)] [[PubMed](#)]
22. Al-Mashreki, M.H.; Eid, M.H.; Saeed, O.; Székács, A.; Szűcs, P.; Gad, M.; Abukhadra, M.R.; AlHammadi, A.A.; Alrakhami, M.S.; Alshabibi, M.A.; et al. Integration of Geochemical Modeling, Multivariate Analysis, and Irrigation Indices for Assessing Groundwater Quality in the Al-Jawf Basin, Yemen. *Water* **2023**, *15*, 1496. [[CrossRef](#)]
23. Ahmed, M.T.; Hasan, M.Y.; Monir, M.U.; Samad, M.A.; Rahman, M.M.; Rifat, M.S.I.; Islam, M.N.; Khan, A.A.; Biswas, P.K.; Jamil, A.N. Evaluation of hydrochemical properties and groundwater suitability for irrigation uses in southwestern zones of Jashore, Bangladesh. *Groundw. Sustain. Dev.* **2020**, *11*, 100441. [[CrossRef](#)]

24. Kouadri, S.; Pande, C.B.; Panneerselvam, B.; Moharir, K.N.; Elbeltagi, A. Prediction of irrigation groundwater quality parameters using ANN, LSTM, and MLR models. *Environ. Sci. Pollut. Res.* **2022**, *29*, 21067–21091. [[CrossRef](#)] [[PubMed](#)]
25. Islam, M.S.; Mostafa, M.G. Development of an integrated irrigation water quality index (IIWQIndex) model. *Water Supply* **2022**, *22*, 2322–2337. [[CrossRef](#)]
26. Khoshneviszadeh, M.; Sakhteman, A. Exploring quantitative structure–activity relationship (QSAR) models for some biologically active catechol structures using PC-LS-SVM and PC-ANFIS. *Appl. Biol. Chem.* **2016**, *59*, 433–441. [[CrossRef](#)]
27. Msaddek, M.H.; Moumni, Y.; Ayari, A.; El May, M.; Chenini, I. Artificial intelligence modelling framework for mapping groundwater vulnerability of fractured aquifer. *Geocarto Int.* **2022**, *37*, 10480–10510. [[CrossRef](#)]
28. Singha, S.; Pasupuleti, S.; Singha, S.S.; Singh, R.; Kumar, S. Prediction of groundwater quality using efficient machine learning technique. *Chemosphere* **2021**, *276*, 130265. [[CrossRef](#)]
29. Lap, B.Q.; Du Nguyen, H.; Hang, P.T.; Phi, N.Q.; Hoang, V.T.; Linh, P.G.; Hang, B.T.T. Predicting water quality index (WQI) by feature selection and machine learning: A case study of An Kim Hai irrigation system. *Ecol. Inform.* **2023**, *74*, 101991. [[CrossRef](#)]
30. El Bilali, A.; Taleb, A.; Brouziye, Y. Groundwater quality forecasting using machine learning algorithms for irrigation purposes. *Agricultural Water Manag.* **2021**, *245*, 106625. [[CrossRef](#)]
31. Ben Alaya, M.; Saidi, S.; Zemni, T.; Zargouni, F. Suitability assessment of deep groundwater for drinking and irrigation use in the Djeffara aquifers (Northern Gabes, south-eastern Tunisia). *Environ. Earth Sci.* **2014**, *71*, 3387–3421. [[CrossRef](#)]
32. Ayari, I.; Ben Alaya, M.; Zammouri, M. Hydrogeochemical characterization and suitability of groundwater for drinking and irrigation in Menzel Bourguiba aquifers (Northeastern Tunisia). *Environ. Monit. Assess.* **2022**, *194*, 524. [[CrossRef](#)] [[PubMed](#)]
33. Najwa Mohd Rizal, N.; Hayder, G.; Mnzool, M.; Elnaim, B.M.E.; Mohammed, A.O.Y.; Khayyat, M.M. Comparison between Regression Models, Support Vector Machine (SVM), and Artificial Neural Network (ANN) in River Water Quality Prediction. *Processes* **2022**, *10*, 1652. [[CrossRef](#)]
34. Haghiahi, A.H.; Nasrolahi, A.H.; Parsaie, A. Water quality prediction using machine learning methods. *Water Qual. Res. J.* **2018**, *53*, 3–13. [[CrossRef](#)]
35. Nadiri, A.A.; Barzegar, R.; Sadeghfam, S.; Rostami, A.A. Developing a Data-Fused Water Quality Index Based on Artificial Intelligence Models to Mitigate Conflicts between GQI and GWQI. *Water* **2022**, *14*, 3185. [[CrossRef](#)]
36. Berhanu, K.G.; Hatiye, S.D.; Lohani, T.K. Coupling support vector machine and the irrigation water quality index to assess groundwater quality suitability for irrigation practices in the Tana sub-basin, Ethiopia. *Water Pract. Technol.* **2023**, *18*, 884–900. [[CrossRef](#)]
37. Chenini, I.; Farhat, B.; Ben Mammou, A. Identification of major sources controlling groundwater chemistry from a multilayered aquifer system. *Chem. Speciat. Bioavailab.* **2010**, *22*, 183–189. [[CrossRef](#)]
38. Ncibi, K.; Mastrocicco, M.; Colombani, N.; Busico, G.; Hadji, R.; Hamed, Y.; Shuhab, K. Differentiating Nitrate Origins and Fate in a Semi-Arid Basin (Tunisia) via Geostatistical Analyses and Groundwater Modelling. *Water* **2022**, *14*, 4124. [[CrossRef](#)]
39. Haji, T.; Zouaghi, T.; Boukadi, N. The role of inherited structures in the evolution of the Meknassy Basin, Central Tunisia, based on geological–geophysical transects. *J. Afr. Earth Sci.* **2014**, *96*, 51–59. [[CrossRef](#)]
40. Msaddek, M.H.; Moumni, Y.; Chenini, I.; Mercier, E.; Dlala, M. Fractures network analysis and interpretation in car-bonate rocks using a multi-criteria statistical approach. Case study of Jebel Chamsi and Jebel Belkhir, South-western part of Tunisia. *J. Afr. Earth Sci.* **2016**, *123*, 99–109. [[CrossRef](#)]
41. Ahmadi, R.; El May, M.; Dlala, M. Ultimate slope design in open pit phosphate mine using geological and geomechanical analysis: Case study of Jebel Jebbeus. *Arab. J. Geosci.* **2019**, *12*, 280. [[CrossRef](#)]
42. Haji, T.A.; Moumni, Y.; Msaddek, M.H. Fault-style analysis and seismic interpretation: Implications for the structural issues of the South-eastern Atlas in Tunisia. *J. Afr. Earth Sci.* **2020**, *172*, 103962. [[CrossRef](#)]
43. Meireles, A.C.M.; Andrade, E.M.D.; Chaves, L.C.G.; Frischkorn, H.; Crisostomo, L.A. A new proposal of the classification of irrigation water. *Rev. Ciéncia Agronómica* **2010**, *41*, 349–357. [[CrossRef](#)]
44. Abbasnia, A.; Yousefi, N.; Mahvi, A.H.; Nabizadeh, R.; Radfar, M.; Yousefi, M.; Alimohammadi, M. Evaluation of groundwater quality using water quality index and its suitability for assessing water for drinking and irrigation purposes: Case study of Sistan and Baluchestan province (Iran). *Hum. Ecol. Risk Assess. Int. J.* **2019**, *25*, 988–1005. [[CrossRef](#)]
45. Leong, W.C.; Bahadori, A.; Zhang, J.; Ahmad, Z. Prediction of water quality index (WQI) using support vector machine (SVM) and least square-support vector machine (LS-SVM). *Int. J. River Basin Manag.* **2021**, *19*, 149–156. [[CrossRef](#)]
46. Tabarak, R.; Khodabakhshi, M.; Fatahi, G. Quantitative structure-critical micelle concentration modeling of anionic gemini surfactants, comparison of MLR, PLS, WNN, and ANFIS models with eigenvalue and correlation ranking methods. *J. Iran. Chem. Soc.* **2021**, *18*, 2703–2711. [[CrossRef](#)]

Disclaimer/Publisher’s Note: The statements, opinions and data contained in all publications are solely those of the individual author(s) and contributor(s) and not of MDPI and/or the editor(s). MDPI and/or the editor(s) disclaim responsibility for any injury to people or property resulting from any ideas, methods, instructions or products referred to in the content.